# Study on the Different Photocatalytic Performances for Tetracycline Hydrochloride Degradation of *p*-block Metal Composite Oxides $Sr_{1.36}Sb_2O_6$ and $Sr_2Sb_2O_7$①

HUANG Yi-Wei[a, b] MAO Jing-Yun[a] QIAN Qing-Rong[a]
XUE Hun[a②] LIU Yan-Ru[b②]

[a] (*College of Environmental Science and Engineering, Fujian Key Laboratory of Pollution Control & Resource Reuse, Fujian Normal University, Fuzhou* 350007, *China*)

[b] (*College of Life Sciences, Fujian Normal University, Fuzhou* 350117, *China*)

**ABSTRACT** *p*-block metal composite oxides $Sr_{1.36}Sb_2O_6$ and $Sr_2Sb_2O_7$ synthesized by a hydrothermal method as photocatalysts in the degradation of tetracycline hydrochloride under UV light irradiation have been extensively studied. The effects of synthesis conditions on the photocatalytic activity were discussed. The $Sr_{1.36}Sb_2O_6$-100 ℃-24 h-5 and $Sr_2Sb_2O_7$-150 ℃-24 h-2 samples prepared under optimal conditions exhibited remarkably different photocatalytic activities. The essential factors influencing the difference of photocatalytic performance were revealed. The results showed that the different photocatalytic activities observed for $Sr_{1.36}Sb_2O_6$ and $Sr_2Sb_2O_7$ could be attributed to their different electronic and crystal structures. Our work will provide a new perspective for the screening and design of p-block metal composite oxide photocatalysts to enhance the removal of organic pollutants in the environment.

**Keywords: *p*-block metal composite oxide, $Sr_{1.36}Sb_2O_6$, $Sr_2Sb_2O_7$, photocatalytic, tetracycline hydrochloride;**
**DOI: 10.14102/j.cnki.0254–5861.2011–3105**

## 1 INTRODUCTION

Recently, the presence of antibiotic residues in water and their harmful effects on ecological environment and human health have aroused worldwide attention. TC (tetracycline hydrochloride) as a kind of antibiotic is usually used in the pharmaceutical industry for humans, animal husbandry and aquaculture to fight infections, which has been considered as one of the most significant pollutants in water environments[1, 2]. Thus, removing TC from water environments by exploiting new control and treatment technologies becomes more and more urgent. Among various elimination methods for TC, semiconductor-based photocatalysis has attracted great attention due to its low energy consumption, high efficiency, nanotoxicity and green advantages[3, 4]. According to previous reports, many semiconductor photocatalysts such as $TiO_2$[5], $Ga_2O_3$[6], $ZnSb_2O_4$[7], ZnO[8], $C_3N_4$[9] and $ZnIn_2S_4$[10] have been used in the removal of TC from wastewater.

It is well-known that *p*-block metal (Sb, In, Ge, Sn, Ga) composite oxides have brought about widespread attention as a class of potential high-efficiency photocatalysts because of its unique crystal and electronic structures[11]. The internal fields as a result of the dipole moment inside the distorted $GeO_4$ tetrahedron or $MO_6$ (M = Sb, In, Sn, or Ga) octahedra and the highly dispersive conduction band due to the hybridization of *s* and *p* orbitals of metal elements may be beneficial to the separation of photogenerated electron-hole pairs[12, 13]. Especially, the antimony composite oxides, like $M_2Sb_2O_7$ (M = Ca or Sr), $MSb_2O_6$ (M = Ca or Zn), $MSbO_3$ (M = Na or Ag), $BiSbO_4$, $Bi_3SbO_7$ and $ZnSb_2O_4$, have been reported to be photocatalysts for water splitting and organic pollutants degradation[14-22]. The valence of Sb ions in most of these compounds is +5. In our previous research, we found that the areal photoactivity of $ZnSb_2O_4$ was remarkably higher than that of $ZnSb_2O_6$[7]. Strontium

Received 20 January 2021; accepted 1 February 2021

① This study was financially supported by the National Natural Science Foundation of China (21875037, 51502036), the National Key Research and Development Program of China (2016YFB0302303, 2019YFC1908203), and the Natural Science Foundation of Distinguished Young Scholars of Fujian Province (2019J06015)

② Corresponding authors. E-mail: xuehun@fjnu.edu.cn or yrliu@fjnu.edu.cn

antimonate composite oxides have many forms including $SrSb_2O_6$, $Sr_{1.36}Sb_2O_6$, $Sr_2Sb_2O_7$, etc. Both $Sr_{1.36}Sb_2O_6$ and $Sr_2Sb_2O_7$ have been reported to be photocatalysts for water splitting[23, 24]. $Sr_2Sb_2O_7$ also exhibits excellent photocatalytic activity in the decomposition of organic pollutants in gas and liquid phase[25]. However, their application for TC degradation has never been explored to the best of our knowledge.

In this study, the performances of $Sr_{1.36}Sb_2O_6$ and $Sr_2Sb_2O_7$ synthesized by a hydrothermal method in the photocatalytic degradation of TC under UV light irradiation were investigated. The influences of synthesis conditions, electronic and crystal structures, specific surface area, and separation of charge carriers on the photocatytic activities of $Sr_{1.36}Sb_2O_6$ and $Sr_2Sb_2O_7$ were systemically studied. The purpose of this study aims to draw a direct correlation between different strontium antimonate composite oxides and their photocatalytic activities, which is of great significance for the screening and design of *p*-block metal composite oxide photocatalyst with improved performance.

## 2 EXPERIMENTAL

### 2. 1 Synthesis

$Sr_{1.36}Sb_2O_6$ and $Sr_2Sb_2O_7$ were synthesized by a hydrothermal method[23, 26]. In a typical procedure, $Sr(CH_3COO)_2$ $0.5H_2O$ (1.07 g, 5.00 mmol), $Sb_2O_5$ (0.81 g, 2.50 mmol) and 70 mL deionized water were added to a 100 mL Teflon-lined stainless-steel autoclave reactor, mechanically stirred for 20 min. The pH of the resulting mixture was adjusted by 4 mol/L nitric acid solution or sodium hydrate solution under constant stirring. The precursor solution was heated at different temperature in an oven for different reaction time. The produced precipitate was washed with distilled water and absolute ethanol for several times and dried in air at 70 ℃. Finally, samples $Sr_{1.36}Sb_2O_6$ or $Sr_2Sb_2O_7$-T-t-n were obtained, where T is the reaction temperature, t the reaction time, and n the pH value or the $OH^-$ concentration of precursor solution (n mol/L).

### 2. 2 Characterization

Phase identifications of $Sr_2Sb_2O_7$ and $Sr_2Sb_{1.36}O_6$ were taken by a Bruker D8 Advance X-ray diffractometer using Cu*Kα* radiation operated at the accelerating voltage of 40 KV and the applied current of 40 mA. Surface morphology of all samples was obtained by scanning electron microscopy (SEM) recorded on a Regulus 8100 field emission (Japan). The transmission electron microscopy (TEM) and high resolution transmission electron microscopy (HRTEM) images were conducted with a JEOL model JEM 2010 EX instrument operated at the accelerating voltage of 200 kV. The light absorption of samples was measured with a Varian Cary 500 UV-vis spectrophotometer (UV-vis DRS) using $BaSO_4$ as the reference. The Brunauer-Emmett-Teller (BET) specific surface area was measured by BELSORP-mini II instrument. Samples were pretreated at 120 $^oC$ for 2 h in vacuum to remove moisture and other gases before the test. Photocurrent measurements were recorded in a three-electrode cell using an electrochemical workstation (Versa STAT3, Princeton Instruments, America). A Pt plate and Ag/AgCl electrode were employed as the counter and reference electrodes, respectively. The working electrode was prepared on fluorine-doped tin oxide (FTO) glass that was cleaned by ultrasonication in ethanol for 30 min. Typically, 5 mg of the photocatalyst was ultrasonicated in 0.5 mL of N,N-dimethylformamide (DMF) to disperse it evenly to get a slurry. After that, the homogeneous paste was spread on the conductive surface of the FTO glass and then dried in air. The electrochemical impedance spectroscopy (EIS) measurements were carried out in the three-electrode cell in the presence of 0.1 M KCl solution containing 10 mM $K_3[Fe(CN)_6]$ under open-circuit potential conditions. ESR signals of the radical spin-trapped by DMPO were examined with a Bruker ESP 300E spectrometer. The settings for the ESR spectrometer were: center field, 3510.00 G; microwave frequency, 9.79 GHz; power, 5.05 mW.

### 2. 3 Photocatalytic activity measurements

The photocatalytic reactions of the samples were performed in a quartz tube with 4.7 cm inner diameter and 16.5 cm length. Four 4W UV lamps with a wavelength centered at 254 nm (Philips, TUV 4W/G4 T5) were equipped as illuminating source. The photocatalyst (150 mg) was added to the vessel containing 150 mL 50 mg/L TC aqueous solution. The mixture was stirred for 1 h in the dark to ensure the establishment of adsorption-desorption equilibrium before irradiation. During irradiation, a 4 mL suspension was collected from the mixture at certain time intervals and centrifuged. The residual contaminant concentration was analyzed by a Shimadzu UV-1750 UV-Vis-NIR spectrophotometer at the detection wavelength of 357 nm.

## 3 RESULTS AND DISCUSSION

In order to obtain the optimal conditions for the hydrothermal synthesis of $Sr_{1.36}Sb_2O_6$ and $Sr_2Sb_2O_7$, the influences of the pH value or the $OH^-$ concentration of precursor solution and the reaction temperature and time on their photocatytic activities were investigated. The XRD patterns of $Sr_{1.36}Sb_2O_6$-180 ℃-24 h-n (n = 1 and 5) synthesized at different pH (Fig. 1a) can be indexed to $Sr_{1.36}Sb_2O_6$ (JCPDS card 81-0735). The UV light-driven photocatalytic activities of $Sr_{1.36}Sb_2O_6$-180 ℃-24 h-n (n = 1 and 5) were explored using the degradation of TC as a model. The temporal concentration changes of TC were monitored by measuring the UV-vis absorption of TC solution at 357 nm to determine the catalytic activities. As shown in Fig. 1b, the photocatalytic activity of $Sr_{1.36}Sb_2O_6$-180 ℃-24 h-5 is higher than that of $Sr_{1.36}Sb_2O_6$-180-24-1. The XRD patterns of $Sr_{1.36}Sb_2O_6$-T ℃-24 h-5 (T = 60, 80, 100, 120, 150) reveals In this survey,we found that a mixture of $Sr_{1.36}Sb_2O_6$ and $Sb_2O_5$ can be obtained at low reaction temperature (60 and 80 ℃) and pure $Sr_{1.36}Sb_2O_6$ is achieved between 100 and 150 ℃ (Fig. 1c). Fig. 1d shows the conversion of TC over $Sr_{1.36}Sb_2O_6$-T ℃-24 h-5 (T = 100, 120 and 150) and $Sr_{1.36}Sb_2O_6$-100 ℃-24 h-5 exhibits the highest photo-catalytic activity for the degradation of TC. The XRD spectrum of $Sr_{1.36}Sb_2O_6$-100 ℃-6 h-5 shows that in addition to the diffraction peaks of $Sr_{1.36}Sb_2O_6$, a diffraction peak attributed to $Sb_2O_5$ appears, indicating that pure $Sr_{1.36}Sb_2O_6$ can not be produced with short reaction time. Pure $Sr_{1.36}Sb_2O_6$ can be formed as the reaction time is more than or equal to 12 h. (Fig. 1e) $Sr_{1.36}Sb_2O_6$-100 ℃-24 h-5 has the best photocatalytic performance and the degradation efficiency of TC over it is found to be 80.7% under UV light irradiation in 180 min (Fig. 1f).

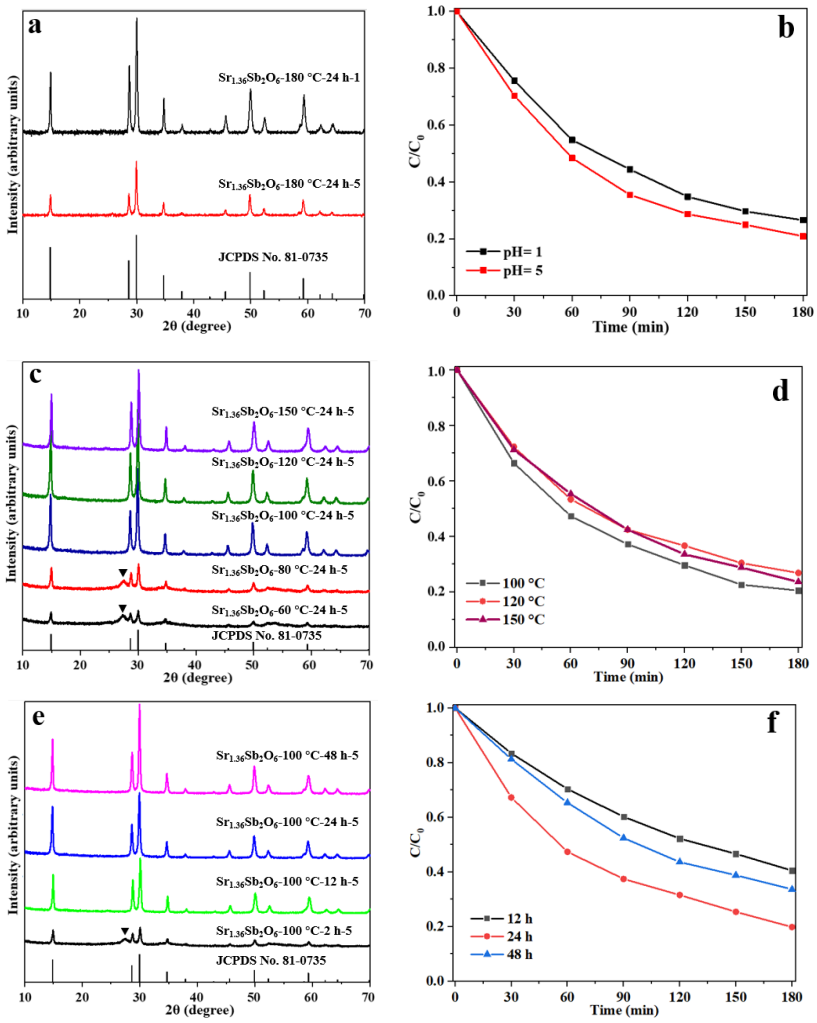


**Fig. 1. XRD patterns of samples: (a) $Sr_{1.36}Sb_2O_6$-180 ℃-24 h-n (n = 1 and 5), (c) $Sr_{1.36}Sb_2O_6$-T ℃-24 h-5 (T = 60, 80, 100, 120, 150), (e) $Sr_{1.36}Sb_2O_6$-100 ℃-t h-5 (t = 2, 12, 24 and 48); Temporal changes of concentration of TC monitored by the UV-vis absorption spectra at 357 nm on samples: (b) $Sr_{1.36}Sb_2O_6$-180 ℃-24 h-n (n = 1 and 5), (d) $Sr_{1.36}Sb_2O_6$-T ℃-24 h-5 (T = 60, 80, 100, 120, 150), (f) $Sr_{1.36}Sb_2O_6$-100 ℃-t h-5 (t = 2, 12, 24 and 48); (▾) $Sb_2O_5$**

Both of the XRD spectra of $Sr_2Sb_2O_7$-180 ℃-24 h-n (n = 1 and 2) obtained with the different $OH^-$ concentration of precursor solution are shown in Fig. 2a. It can be observed that both samples are in good agreement with the phase of $Sr_2Sb_2O_7$ (JCPDS card 78-1774). Compared with $Sr_2Sb_2O_7$-180 ℃-24 h-1, $Sr_2Sb_2O_7$-180 ℃-24 h-2 exhibits enhanced degradation efficiency (Fig. 2b). Fig. 2c shows the XRD patterns of the $Sr_2Sb_2O_7$-T ℃-24 h-2 (T = 100, 120, 150, 180 and 200). All the diffraction peaks can be indexed to pure $Sr_2Sb_2O_7$. The photocatalytic degradation efficiency of the samples obtained at different reaction temperature follows the sequence: 150 ℃ > 180 ℃ > 200 ℃ > 120 ℃ > 100 ℃ (Fig. 2d). Fig. 2e shows the XRD patterns of the as-prepared $Sr_2Sb_2O_7$-150 ℃-t h-2 (t = 6, 12, 24 and 36) with different reaction time. When the reaction time is 6 h, a mixture of $Sr_2Sb_2O_7$ and $Sb_2O_5$ can be obtained. With the reaction time over or equal to 12 h, no obvious diffraction peaks of impure phases are found, indicating the high purity of as-prepared $Sr_2Sb_2O_7$ samples. The results of TC degradation over $Sr_2Sb_2O_7$-150 ℃-t h-2 (t = 12, 24 and 36) are given in Fig. 2f. $Sr_2Sb_2O_7$-150 ℃-24 h-2 displays the highest photocatalytic activity and 99.7% of TC is removed after 30 min UV light irradiation.

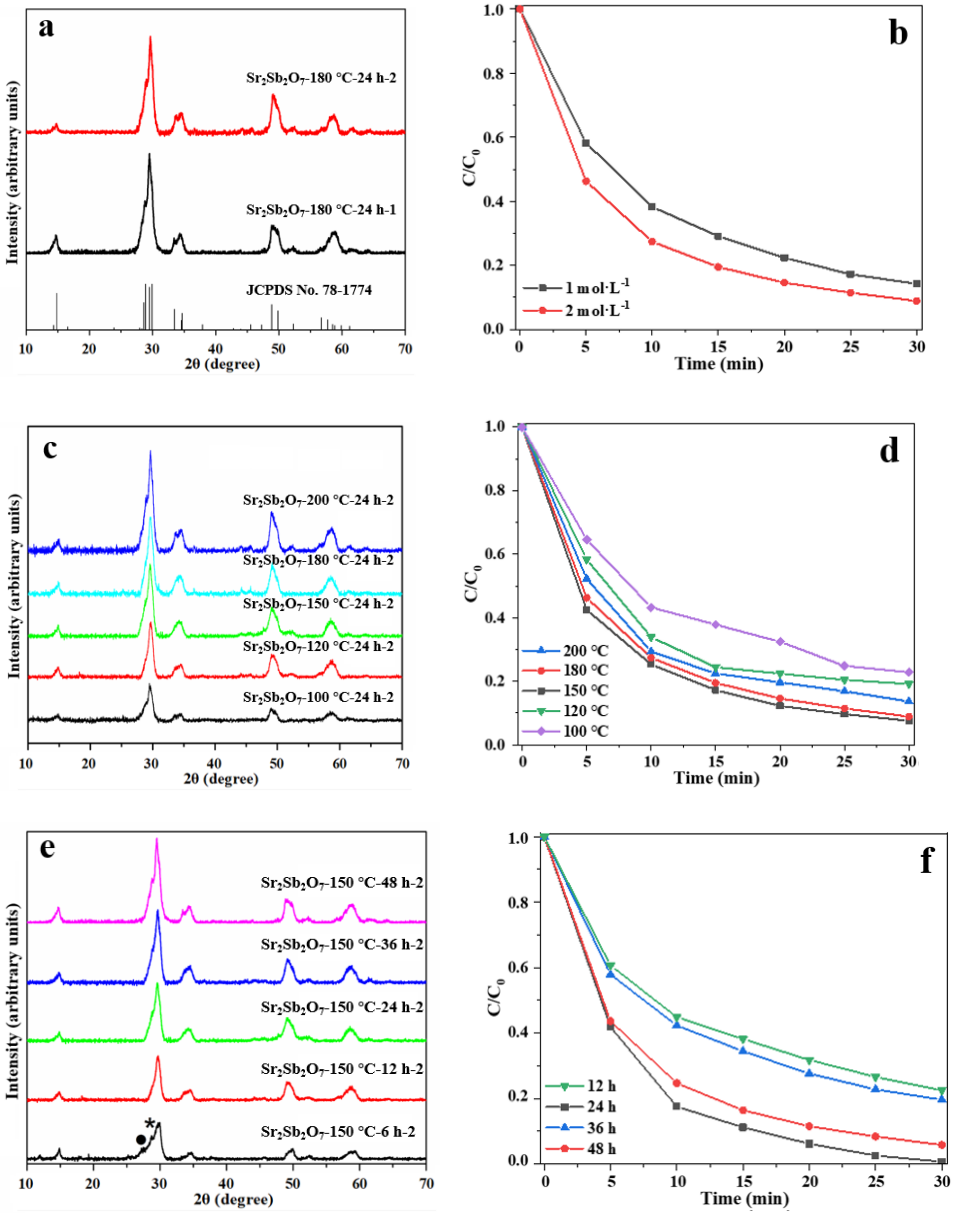


**Fig. 2. XRD patterns of samples: (a) $Sr_2Sb_2O_7$-180 ℃-24 h-n (n = 1 and 2), (c) $Sr_2Sb_2O_7$-T ℃-24 h-2 (T = 100, 120, 150, 180 and 200), (e) $Sr_2Sb_2O_7$-150 ℃-t h-2 (t = 6, 12, 24 and 36); Temporal changes of concentration of TC monitored by the UV-vis absorption spectra at 357 nm on samples: (b) $Sr_2Sb_2O_7$-180 ℃-24 h-n (n = 1 and 2), (d) $Sr_2Sb_2O_7$-T ℃-24 h-2 (T = 100, 120, 150, 180 and 200), (f) $Sr_2Sb_2O_7$-150 ℃-t h-2 (t = 6, 12, 24 and 36); (●) $Sb_2O_5$, (*) $Sr(OH)_2$**

Based on the above results, the optimal conditions for the hydrothermal synthesis of $Sr_{1.36}Sb_2O_6$ and $Sr_2Sb_2O_7$ are determined to be: the pH value 5 and the $OH^-$ concentration of precursor solution 2 mol/L, hydrothermal temperature 100 and 150 ℃, reaction time 5 and 24 h, respectively. The $Sr_{1.36}Sb_2O_6$-100 ℃-24 h-5 and $Sr_2Sb_2O_7$-150 ℃-24 h-2 samples prepared under optimal conditions exhibit a remarkably different photocatalytic activity for the degradation of TC. In order to reveal the relationship between composition, structure and photocatalytic performance, the morphology, surface areas, optical absorption property, the main active species in photocatalytic reaction, the charge carriers' transfer and separation behaviors, electronic and crystal structures of $Sr_{1.36}Sb_2O_6$ and $Sr_2Sb_2O_7$ prepared under optimal conditions are characterized systematically.

The morphology and microstructures of $Sr_{1.36}Sb_2O_6$ and $Sr_2Sb_2O_7$ were investigated by SEM, TEM and HRTEM, respectively. In the SEM image in Fig. 3a, the as-prepared $Sr_{1.36}Sb_2O_6$ consists entirely of octahedra with diameters of 30～80 nm. This indicates that the octahedra can be successfully synthesized on a large scale. The average diameter of the octahedra, measured in a typical TEM image of $Sr_{1.36}Sb_2O_6$ (Fig. 3b), is approximately 50 nm. In the HRTEM image (Fig. 3c), the clear lattice fringes indicate the good crystallization of $Sr_{1.36}Sb_2O_6$. The spacing of the lattice fringes is 0.30 nm, which means that they belong to the (222) plane of $Sr_{1.36}Sb_2O_6$. The typical SEM image of $Sr_2Sb_2O_7$ (Fig. 3d) shows that the sample consists of small particles. The TEM image of $Sr_2Sb_2O_7$ is shown in Fig. 3e, which indicates that the average size of nanoparticles is around 9 nm. Clear diffraction patterns with interdistance d = 0.30 nm can be seen in the HRTEM image of the sample (Fig. 3f), which corresponds to the (220) plane of $Sr_2Sb_2O_7$. Additionally, the crystallite size of $Sr_{1.36}Sb_2O_6$ is much larger than that of $Sr_2Sb_2O_7$, which may lead to the significantly different BET surface areas. The specific surface areas of the samples are determined with the $N_2$ absorption-desorption isotherm curves (Fig. 4). The BET specific surface area of $Sr_2Sb_2O_7$ is 29.6 $m^2\ g^{-1}$, which is 1.6 times larger than that of $Sr_{1.36}Sb_2O_6$ (18.9 $m^2\ g^{-1}$). However, the photocatalytic performance of $Sr_2Sb_2O_7$ is much better than that of $Sr_{1.36}Sb_2O_6$, indicating the specific surface area is not the main factor affecting their photocatalytic activity.

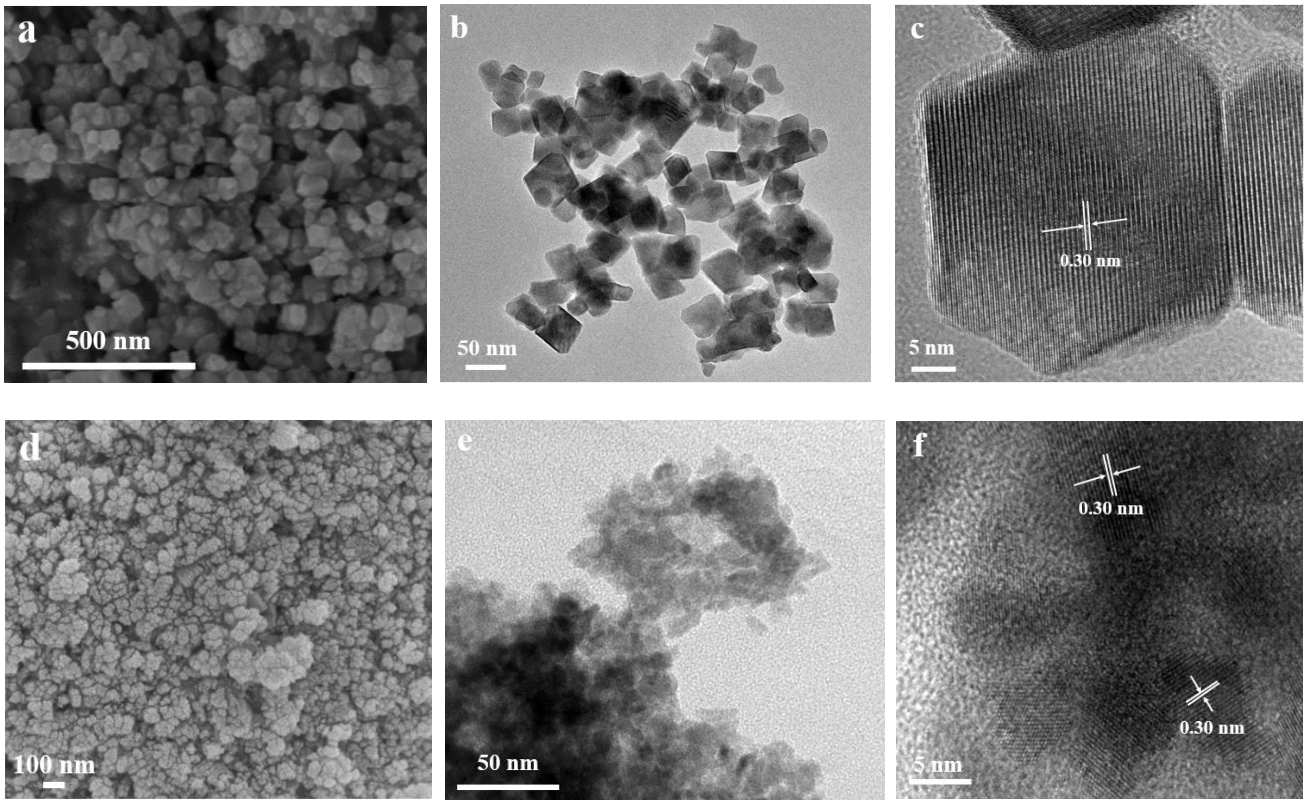


**Fig. 3. Images of the $Sr_{1.36}Sb_2O_6$-100 ℃-24 h-5 sample: (a) SEM image; (b) TEM image; (c) HRTEM image; Images of the $Sr_2Sb_2O_7$-150 ℃-24 h-2 sample: (d) SEM image; (e) TEM image; (f) HRTEM image**

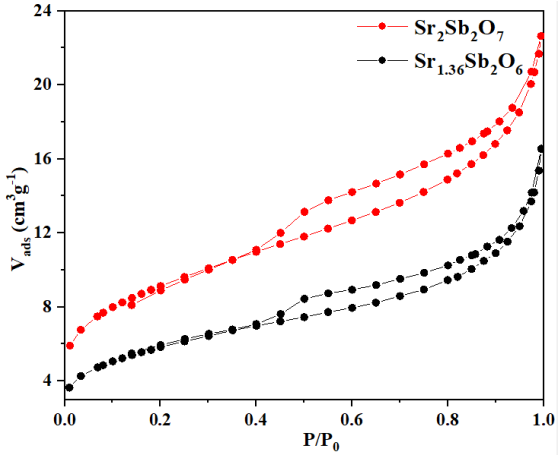


**Fig. 4. Nitrogen adsorption-desorption isotherm for $Sr_{1.36}Sb_2O_6$-100 ℃-24 h-5 and $Sr_2Sb_2O_7$-150 ℃-24 h-2**

The UV-vis diffuse reflectance spectroscopy of $Sr_{1.36}Sb_2O_6$ and $Sr_2Sb_2O_7$ is shown in Fig. 5. The absorptions for $Sr_{1.36}Sb_2O_6$ and $Sr_2Sb_2O_7$ locate at ca. 292 and 323 nm, corresponding to a band gap of about 4.2 and 3.8 eV, respectively. It is well known that the wide band gap endows the photogenerated holes and electrons with strong redox ability[27, 28]. $Sr_{1.36}Sb_2O_6$ has a small band gap energy compared with $Sr_2Sb_2O_7$, and thus it possesses lower photocatalytic activity.

To testify the active species involved in different photocatalytic systems, EPR spin trap technique was carried out. As shown in Fig. 6, the typical peaks of DMPO-OH• and DMPO-$O_2^-$• under the UV light irradiation are observed. The generation amount of OH• and $O_2^-$• in $Sr_2Sb_2O_7$ system is more than that in $Sr_{1.36}Sb_2O_6$, which may be one of the reasons for the higher photocatalytic degradation efficiency[29-31].

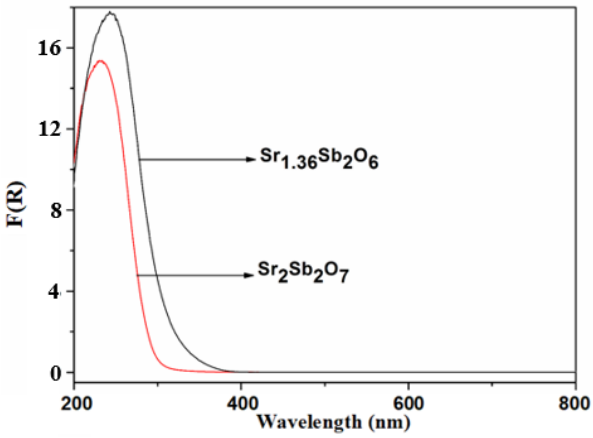


**Fig. 5. Diffuse reflectance absorption spectra of $Sr_{1.36}Sb_2O_6$-100 ℃-24 h-5 and $Sr_2Sb_2O_7$-150 ℃-24 h-2**

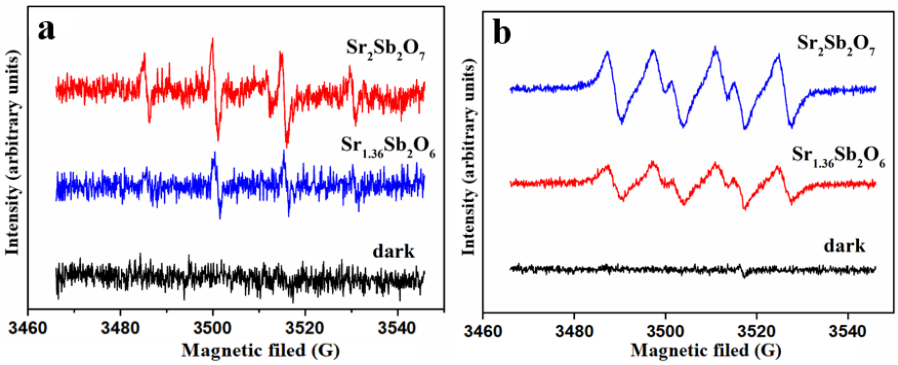


**Fig. 6. ESR signals of DMPO-trapped •OH for $Sr_{1.36}Sb_2O_6$-100 ℃-24 h-5 and $Sr_2Sb_2O_7$-150 ℃-24 h-2**

The charge carriers' transfer and separation behaviors were investigated by the photoelectrochemical properties. As the photocurrent response curves and EIS Nyquist plots of $Sr_{1.36}Sb_2O_6$ and $Sr_2Sb_2O_7$ shown in Fig. 7, $Sr_2Sb_2O_7$ shows stronger photocurrent density and smaller EIS arc radius than $Sr_{1.36}Sb_2O_6$, indicating higher charge transfer and separation efficiency on the surface of $Sr_2Sb_2O_7$, which leads to the higher photocatalytic performance[32, 33].

The activity of a photocatalyst is closely related to the distorted tetrahedral or octahedral units in its crystal structure[34, 35]. In our previous study we found that the different photocatalytic activities of $ZnSb_2O_4$ and $ZnSb_2O_6$ were strongly associated with their crystal structures, and the distortion of $SbO_3$ tetrahedra in $ZnSb_2O_4$ contributed to its high photocatalytic activity[7]. Fig. 8 shows the schematic representation of $Sr_{1.36}Sb_2O_6$ and $Sr_2Sb_2O_7$ structures. The $SbO_6$ tetrahedra in $Sr_{1.36}Sb_2O_6$ crystal are composed of six Sb–O bonds with the same bond length (Sb–O, 1.974 Å×6). However, there are two kinds of distorted Sb–O octahedra in $Sr_2Sb_2O_7$ crystal. One is the stretched $SbO_6$ octahedra which are composed of two long and four short Sb–O bonds (Sb–O: 2.005 Å×2, Sb–O: 1.971 Å×4), and the other is the flattened $SbO_6$ octahedra made up of two short and four long Sb–O bonds (Sb–O: 1.922 Å×2, Sb–O: 2.021 Å×4). We think that the distortion of $SbO_6$ octahedra is the main reason for the remarkable difference of photocatalytic activity between $Sr_{1.36}Sb_2O_6$ and $Sr_2Sb_2O_7$. The internal electric field formed by dipole moment of distorted $SbO_6$ octahedra can be helpful to the separation of electron and hole, thus leading to the improvement of photocatalytic activity.

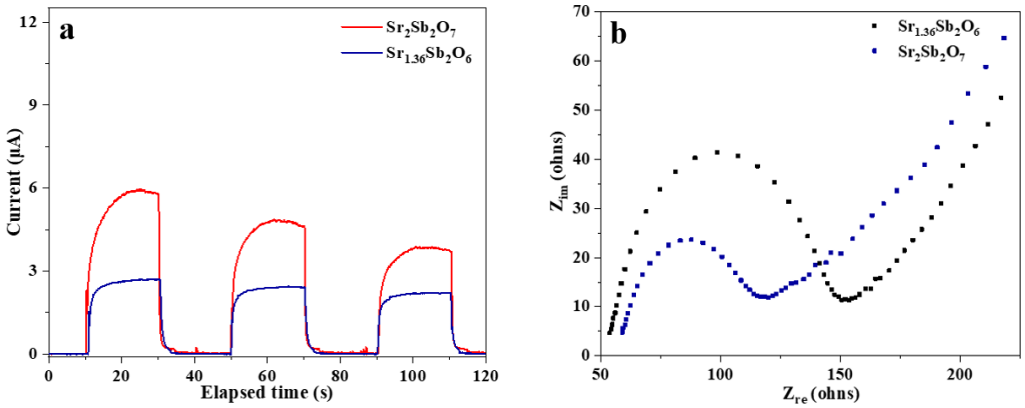


**Fig. 7. (a) Photocurrents, (b) Electrochemical impedance spectroscopy (EIS) Nynquist plots of $Sr_{1.36}Sb_2O_6$-100 ℃-24 h-5 and $Sr_2Sb_2O_7$-150 ℃-24 h-2**

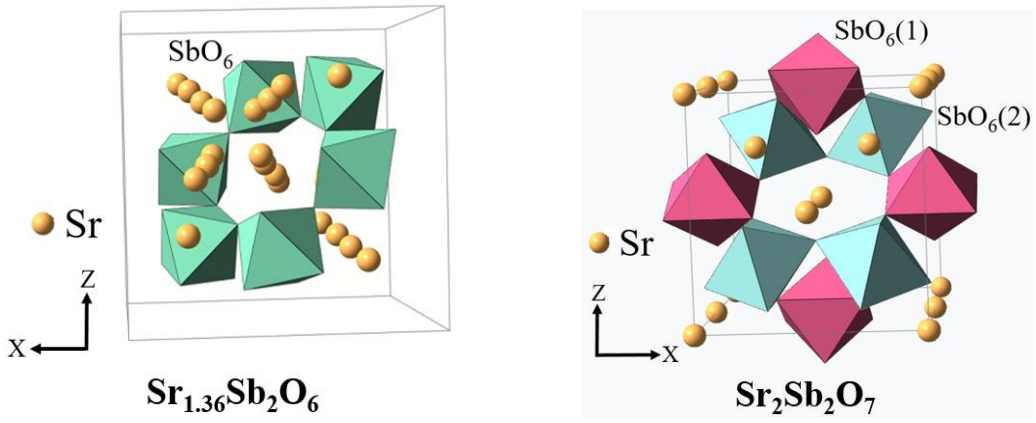


**Fig. 8. Schematic representation of $Sr_{1.36}Sb_2O_6$ and $Sr_2Sb_2O_7$ crystal structures**

## 4 CONCLUSION

In the present work, *p*-block metal composite oxides $Sr_{1.36}Sb_2O_6$ and $Sr_2Sb_2O_7$ synthesized by a hydrothermal method were applied to TC photocatalytic degradation for the first time. The $Sr_{1.36}Sb_2O_6$-100 ℃-24 h-5 and $Sr_2Sb_2O_7$-150 ℃-24 h-2 samples prepared under optimal conditions exhibited remarkably different photocatalytic activities. The degradation efficiency of TC over $Sr_{1.36}Sb_2O_6$-100 ℃-24 h-5 was found to be 80.7% in 180

min and 99.7% of TC was removed in 30 min using $Sr_2Sb_2O_7$-150 ℃-24 h-2 as a photocatalyst under UV light irradiation. The difference of photocatalytic performance between $Sr_{1.36}Sb_2O_6$ and $Sr_2Sb_2O_7$ was mainly attributed to their different electronic and crystal structures that led to the differences on the redox ability of photogenerated holes and electrons, charges transfer and separation efficiency, and generation amount of active species. Our work will facilitate the development of novel semiconductor photocatalytic materials using *p*-block metal composite oxides for organic pollutants degradation.

## REFERENCES


(1) Xu, L. Y.; Zhang, H.; Xiong, P.; Zhu, Q. Q.; Liao, C. Y.; Jiang, G. B. Occurrence, fate, and risk assessment of typical tetracycline antibiotics in the aquatic environment: a review. *Sci. Total. Environ*. **2020**, 141975–141975.

(2) Dai, Y. J.; Liu, M.; Li, J. J.; Yang, S. S.; Sun, Y.; Sun, Q. Y.; Wang, W. S.; Lu, L.; Zhang, K. X.; Xu, J. Y.; Zheng, W. L.; Hu, Z. Y.; Yang, Y. H.; Gao, Y. W.; Liu, Z. H. A review on pollution situation and treatment methods of tetracycline in groundwater. *Sep. Sci. Technol.* **2020**, 55, 1005–1021.

(3) Rasheed, H. U.; Lv, X. M.; Wei, W.; Sam, D. K.; Ullah, N.; Xie, J. M.; Zhu, W. H. Highly efficient photocatalytic degradation of the tetracycline hydrochloride on the alpha-$Fe_2O_3$@CN composite under the visible light. *J. Environ. Chem. Eng*. **2019**, 7, 103322.

(4) Li, W.; Ding, H.; Ji, H.; Dai, W. B.; Guo, J. P.; Du, G. X. Photocatalytic degradation of tetracycline hydrochloride via a CdS-$TiO_2$ heterostructure composite under visible light irradiation. *Nanomaterials* **2018**, 8, 415.

(5) Wu, S. Q.; Hu, H. Y.; Lin, Y.; Zhang, J. L.; Hu, Y. H. Visible light photocatalytic degradation of tetracycline over $TiO_2$. *Chem. Eng. J.* **2020**, 382, 122842.

(6) Zeng, L. X.; Wang, J. Q.; Qian, Q. R.; Chen, Q. H.; Liu, X. P.; Luo, Y. J.; Xue, H.; Li, Z. H. Photocatalytic degradation of tetracycline hydrochloride over rugby-like beta-$Ga_2O_3$ with a 3D hierarchically assembled porous structure for environmental remediation. *Catal. Sci. Technol.* **2020**, 10, 3315–3323.

(7) Xue, H.; Liao, S. X.; Chen, Y. L.; Qian, Q. R.; Liu, X. P.; Chen, Q. H. Application and mechanism of $ZnSb_2O_4$ and $ZnSb_2O_6$ in the photocatalytic degradation of tetracycline hydrochloride. *Chin. J. Struct. Chem.* **2019**, 38, 837–847.

(8) Lwin, H. M.; Zhan, W. Q.; Song, S. X.; Jia, F. F.; Zhou, J. B. Visible-light photocatalytic degradation pathway of tetracycline hydrochloride with cubic structured ZnO/$SnO_2$ heterojunction nanocatalyst. *Chem. Phys. Lett.* **2019**, 736, 136806.

(9) Rasheed, H. U.; Lv, X. M.; Wei, W.; Yaseen, W.; Ullah, N.; Xie, J. M.; Zhu, W. H. Synthesis and studies of ZnO doped with g-$C_3N_4$ nanocomposites for the degradation of tetracycline hydrochloride under the visible light irradiation. *J. Environ. Chem. Eng.* **2019**, 7, 103152.

(10) Chen, W.; Chang, L.; Ren, S. B.; He, Z. C.; Huang, G. B.; Liu, X. H. Direct Z-scheme 1D/2D $WO_{2.72}$/$ZnIn_2S_4$ hybrid photocatalysts with highly-efficient visible-light-driven photodegradation towards tetracycline hydrochloride removal. *J. Hazard. Mater.* **2020**, 384, 121308.

(11) Inoue, Y. Photocatalytic water splitting by $RuO_2$-loaded metal oxides and nitrides with $d^0$- and $d^{10}$-related electronic configurations. *Energy Environ. Sci.* **2009**, 2, 364–386.

(12) Kadowaki, H.; Sato, J.; Kobayashi, H.; Saito, N.; Nishiyama, H.; Simodaira, Y.; Inoue, Y. Photocatalytic activity of the $RuO_2$-dispersed composite *p*-block metal oxide $LiInGeO_4$ with $d^{10}$-$d^{10}$ configuration for water decomposition. *J. Phys. Chem. B* **2005**, 109, 22995–23000.

(13) Sato, J.; Kobayashi, H.; Ikarashi, K.; Saito, N.; Nishiyama, H.; Inoue, Y. Photocatalytic activity for water decomposition of $RuO_2$-dispersed $Zn_2GeO_4$ with $d^{10}$ configuration. *J. Phys. Chem. B* **2004**, 108, 4369–4375.

(14) Chen, L. C.; Cui, W.; Li, J. Y.; Wang, H.; Dong, X. A.; Chen, P.; Zhou, Y.; Dong, F. The high selectivity for benzoic acid formation on $Ca_2Sb_2O_7$ enables efficient and stable toluene mineralization. *Appl. Catal. B-Environ.* **2020**, 118948.

(15) Huang, R. K.; Xu, X. M.; Zhu, J.; Liu, W. J.; Yuan, R. S.; Fu, X. Z.; Zhang, Y. F.; Li, Z. H. Nanocrystalline $CaSb_2O_5(OH)_2$ and $Ca_2Sb_2O_7$: controlled syntheses, electronic structures and photocatalytic activity. *Appl. Catal. B-Environ.* **2012**, 127, 205–211.

(16) Zhang, M.; Chen, L. M.; Yao, S. Y.; Long, Y. M.; Li, W. F.; Wang, Z. S. Effect of calcination temperature on the photocatalytic activity of $CaSb_2O_6$ nanoparticles prepared by co-precipitation method. *Catal. Commun.* **2014**, 48, 29–32.

(17) Li, G. Q.; Wang, W. L.; Yang, N.; Zhang, W. F. Composition dependence of $AgSbO_3$/$NaNbO_3$ composite on surface photovoltaic and visible-light photocatalytic properties. *Appl. Phys. a-Mater.* **2011**, 103, 251–256.

(18) Sato, J.; Saito, N.; Nishiyama, H.; Inoue, Y. Photocatalytic water decomposition by $RuO_2$-loaded antimonates, $M_2Sb_2O_7$ (M = Ca, Sr), $CaSb_2O_6$ and $NaSbO_3$, with $d^{10}$ configuration. *J. Photoch. Photobio. A* **2002**, 148, 85–89.

(19) Liu, W. J.; Lin, P. Y.; Jin, H.; Xue, H.; Zhang, Y. F.; Li, Z. H. Nanocrystalline $ZnSb_2O_6$: hydrothermal synthesis, electronic structure and

photocatalytic activity. *J. Mol. Catal. a-Chem.* **2011**, 349, 80–85.

(20) Lin, X. P.; Huang, F. Q.; Wang, W. D.; Zhang, K. L. A novel photocatalyst $BiSbO_4$ for degradation of methylene blue. *Appl. Catal. a-Gen.* **2006**, 307, 257–262.

(21) Lin, X. P.; Huang, F. Q.; Wang, W. D.; Shan, Z. C.; Shi, J. L. Methyl orange degradation over a novel Bi-based photocatalyst $Bi_3SbO_7$: correlation of crystal structure to photocatalytic activity. *Dyes. Pigments* **2008**, 78, 39–47.

(22) Kako, T.; Kikugawa, N.; Ye, J. Photocatalytic activities of $AgSbO_3$ under visible light irradiation. *Catal. Today* **2008**, 131, 197–202.

(23) Xue, H.; Chen, Y. Y.; Ding, N.; Chen, Q. H.; Luo, Y. J.; Liu, X. P.; Xiao, L. R.; Qian, Q. R. Hydrothermal synthesis of $Sr_{1.36}Sb_2O_6$ nano-octahedra with photocatalytic activity for overall splitting of water. *Catal. Commun.* **2016**, 74, 5–9.

(24) Xue, H.; Li, Z.; Wu, L.; Ding, Z.; Wang, X.; Fu, X. Nanocrystalline ternary wide band gap *p*-block metal semiconductor $Sr_2Sb_2O_7$: hydrothermal syntheses and photocatalytic benzene degradation. *J. Phys. Chem. C* **2008**, 112, 5850–5855.

(25) Xue, H.; Li, Z. H.; Dong, H.; Wu, L.; Wang, X. X.; Fu, X. Z. 3D hierarchical architectures of $Sr_2Sb_2O_7$: hydrothermal syntheses, formation mechanisms, and application in aqueous-phase photocatalysis. *Cryst. Growth. Des.* **2008**, 8, 4469–4475.

(26) Li, Z. H.; Liu, P.; Fu, X. Z. Wide bandgap *p*-block metal oxides/hydroxides for photocatalytic benzene degradation. *Acta Phys-Chim. Sin.* **2010**, 26, 877–884.

(27) Chen, X.; Xue, H.; Li, Z. H.; Wu, L.; Wang, X. X.; Fu, X. Z. Ternary wide band gap p-block metal semiconductor $ZnGa_2O_4$ for photocatalytic benzene degradation. *J. Phys. Chem. C* **2008**, 112, 20393–20397.

(28) Emeline, A.; Kataeva, G. V.; Litke, A. S.; Rudakova, A. V.; Ryabchuk, V. K.; Serpone, N. Spectroscopic and photoluminescence studies of a wide band gap insulating material: powdered and colloidal $ZrO_2$ sols. *Langmuir*. **1998**, 14, 5011–5022.

(29) Pare, B.; Jonnalagadda, S. B.; Tomar, H.; Singh, P.; Bhagwat, V. W. ZnO assisted photocatalytic degradation of acridine orange in aqueous solution using visible irradiation. *Desalination* **2008**, 232, 80–90.

(30) Sun, M.; Li, D.; Zhang, W.; Fu, X.; Shao, Y.; Li, W.; Xiao, G.; He, Y. Rapid microwave hydrothermal synthesis of GaOOH nanorods with photocatalytic activity toward aromatic compounds. *Nanotechnology* **2010**, 21, 355601.

(31) Liu, T. T.; Wang, L.; Lu, X.; Fan, J. M.; Cai, X. X.; Gao, B.; Miao, R.; Wang, J. X.; Lv, Y. T. Comparative study of the photocatalytic performance for the degradation of different dyes by $ZnIn_2S_4$: adsorption, active species, and pathways. *Rsc. Adv.* **2017**, 7, 12292–12300.

(32) Lv, Y. H.; Zhu, Y. Y.; Zhu, Y. F. Enhanced photocatalytic performance for the $BiPO_4$-*x* nanorod induced by surface oxygen vacancy. *J. Phys. Chem. C* **2013**, 117, 18520–18528.

(33) Deng, Y. C.; Tang, L.; Zeng, G. M.; Feng, C. Y.; Dong, H. R.; Wang, J. J.; Feng, H. P.; Liu, Y. N.; Zhou, Y. Y.; Pang, Y. Plasmonic resonance excited dual Z-scheme $BiVO_4$/Ag/$Cu_2O$ nanocomposite: synthesis and mechanism for enhanced photocatalytic performance in recalcitrant antibiotic degradation. *Environ. Sci-Nano*. **2017**, 4, 1494–1511.

(34) Sato, J.; Kobayashi, H.; Inoue, Y. Photocatalytic activity for water decomposition of indates with octahedrally coordinated $d^{10}$ configuration. *J. Phys. Chem. B* **2003**, 107, 7970–7975.

(35) Li, G.; Dimitrijevic, N. M.; Chen, L.; Nichols, J. M.; Rajh, T.; Gray, K. A. The important role of tetrahedral $Ti^{4+}$ sites in the phase transformation and photocatalytic activity of $TiO_2$ nanocomposites. *J. Am. Chem. Soc*. **2008**, 130, 5402–5403.